Increased Equivalent Input Noise in Glaucomatous Central Vision: Is it Due to Undersampling of Retinal Ganglion Cells?

Rong Liu and MiYoung Kwon

Department of Ophthalmology and Visual Sciences, School of Medicine, University of Alabama at Birmingham, Birmingham, Alabama, United States

Correspondence: MiYoung Kwon, Department of Ophthalmology and Visual Sciences, School of Medicine, The University of Alabama at Birmingham, 700 S. 18th Street, Suite 415, Birmingham, AL 35294-0009, USA; kwon@uab.edu.

Received: January 30, 2020
Accepted: June 1, 2020
Published: July 9, 2020

Citation: Liu R, Kwon M. Increased equivalent input noise in glaucomatous central vision: is it due to undersampling of retinal ganglion cells?. *Invest Ophthalmol Vis Sci.* 2020;61(8):10. https://doi.org/10.1167/iovs.61.8.10

Purpose. Recent evidence shows that macular damage is common even in early stages of glaucoma. Here we investigated whether contrast sensitivity loss in the central vision of glaucoma patients is due to an increase in equivalent input noise (N_{eq}), a decrease in calculation efficiency, or both. We also examined how retinal undersampling resulting from loss of retinal ganglion cells (RGCs) may affect N_{eq} and calculation efficiency.

Methods. This study included 21 glaucoma patients and 23 age-matched normally sighted individuals. Threshold contrast for orientation discrimination was measured with a sinewave grating embedded in varying levels of external noise. Data were fitted to the linear amplifier model (LAM) to factor contrast sensitivity into N_{eq} and calculation efficiency. We also correlated macular RGC counts estimated from structural (spectral-domain optical coherence tomography) and functional (standard automated perimetry Swedish interactive thresholding algorithm 10-2) data with either N_{eq} or efficiency. Furthermore, using analytical and computer simulation approach, the relative effect of retinal undersampling on N_{eq} and efficiency was evaluated by adding the RGC sampling module into the LAM.

Results. Compared with normal controls, glaucoma patients exhibited a significantly larger N_{eq} without significant difference in efficiency. N_{eq} was significantly correlated with Pelli-Robson contrast sensitivity and macular RGC counts. The results from analytical derivation and model simulation further demonstrated that N_{eq} can be expressed as a function of internal noise and retinal sampling.

Conclusions. Our results showed that equivalent input noise is significantly elevated in glaucomatous vision, thereby impairing foveal contrast sensitivity. Our findings further elucidated how undersampling at the retinal level may increase equivalent input noise.

Keywords: retinal ganglion cell, contrast sensitivity, equivalent input noise, calculation efficiency, undersampling, internal noise, glaucoma, optical coherence tomography, retinal layer thickness

Glaucoma, characterized by a progressive loss of retinal ganglion cells (RGCs) and the associated visual field defects,[1–3] is a leading cause of blindness worldwide. Primary open angle glaucoma, the most common type of glaucoma, is known for peripheral vision loss as central vision loss often occurs at the end stage. Accumulating evidence, however, has shown that glaucomatous damage involves the macular region even in the early stages. For example, a number of imaging studies[4,5] have reported that the thickness of RGC plus inner plexiform (RGC+) layer (where the ganglion cell bodies and their dendritic structures are located) is significantly thinner in the macula of early glaucomatous eyes compared with age-matched healthy eyes. RGCs are the output neurons of the human retina and the first stage in which visual sensory information is encoded as spikes, placing a fundemental constraint on cortical visual processing.[6] Consistent with anatomical evidence, behavioral measurements also indicate that central visual functions deteriorate in glaucoma.[7–11] Particularly, despite normal visual acuity, foveal contrast sensitivity was found to be significantly impaired even in early stages of glaucoma compared with normal cohorts.[12–16] Contrast sensitivity, the ability to detect differences in contrast, is a fundamental building block of human pattern vision, and thus affects a wide range of everyday visual functions, such as reading,[17–19] object/face recognition,[20,21] gait,[19,22] and driving[23,24] (also see a review[25]). Contrast information (i.e., the intensity difference between the light and dark regions of visual space) is first encoded in center-surround RGCs[26] and further processed in the downstream cortical areas. Thus identifying the mechanism underlying foveal contrast sensitivity loss in glaucoma is important for us to understand not

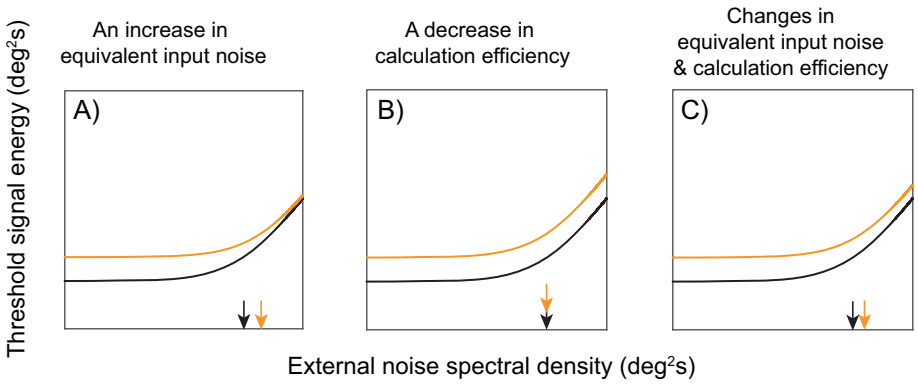

Figure 1. Three hypothetical outcomes shown by threshold versus noise curves. The threshold signal energy required for target discrimination is plotted as a function of external noise spectral density on log-log coordinates. The *black line* represents the hypothetical curve of normal vision, whereas the *orange line* indicates that of glaucomatous vision. The *arrows* on the horizontal axis represent the corresponding equivalent input noise level. (**A**) An increase in equivalent input noise without any change in calculation efficiency. Threshold energy is elevated predominately at low noise levels. (**B**) A decrease in calculation efficiency without any change in equivalent input noise. Threshold energy is elevated across all noise levels (i.e., a vertical upward shift of the curve). (**C**) Changes in both equivalent input noise and calculation efficiency: an increase in equivalent input noise and a decrease in calculation efficiency.

only functional deficits occurring in glaucomatous central vision, but also the way RGC damage undermines human pattern vision.

Contrast sensitivity is often measured without external noise as shown in Pelli-Robson or CSV-1000 contrast sensitivity charts. However, by measuring contrast sensitivity in the presence of external noise, one can identify the mechanism underlying a loss of contrast sensitivity. As illustrated in Figure 1, a person's contrast thresholds can be measured as a function of external noise level, which allows us to partition the limiting factor into two major quantities: equivalent input noise and calculation efficiency. Equivalent input noise represents changes in internal noise[27] due to optical and/or neural factors (see review[28]), whereas calculation efficiency (also termed sampling efficency) represents how efficiently the human observer extracts the information available in stimulus relative to an ideal observer. Thus any changes in computations made in the decision-making process, such as template matching,[29,30] integration properties,[31,32] or decision-making strategies, will likely affect calculation efficiency. This method is called equivalent input noise paradigm,[28,29] as it enables us to gauge the external noise level equivalent to the level of internal noise in the system. This paradigm has been employed in a number of studies that aim to elucidate the mechanism underpinning changes in contrast sensitivity due to either aging,[33–37] perceptual learning,[38–40] spatial attention,[41] or stimulus properties, such as spatial frequency.[42–44] The equivalent input noise paradigm has been also used to characterize a loss of contrast sensitivity in various clinical populations, including amblyopia,[45–47] retinitis pigmentosa,[48] diabetes,[49] schizophrenia,[50] and dyslexia.[51] It was also used to study the mechanism underlying a loss of motion sensitivity in glaucoma.[52]

In the current study, we adopted this equivalent input noise paradigm to determine whether contrast sensitivity loss in the central vision of glaucoma patients is a result of an increase in equivalent input noise, a decrease in calculation efficiency, or both. Here we have three hypothetical outcomes: first, if it were the case in which equivalent input noise increases without any change in calculation efficiency, then contrast thresholds would be elevated at low noise levels but not at high noise levels as shown by the orange curve plotted on log-log coordinates (Fig. 1A). Second, if it were the case in which calculation efficiency decreases without any change in equivalent input noise, then contrast thresholds would be elevated across all noise levels, resulting in a vertical upward shift of the curve as shown by the orange line in Figure 1B. Third, if it were the case in which both an increase in equivalent input noise and a reduction in calculation efficicency take place, then the result would be as depicted by the orange line in Figure 1C.

We further examined optical and neural factors that might account for the increase or decrease in equivalent input noise and/or calculation efficiency. Using both analytical derivation and computer model simulation, we also elucidated how retinal undersampling resulting from ganglion cell damage may affect equivalent input noise and calculation efficiency. We acknowlege that the term "sampling" can refer to a sampling strategy involved in perceptual decision-making, as well as the sampling density of retinal neurons given the fact the dendritic fields of either photoreceptors or ganglion cells tile the entire visual space.[53–55] To avoid confusion, the term "calculation efficiency" instead of "sampling efficiency" is used to refer to the sampling process at a higher-level decision-making stage, whereas the term "undersampling" is used to refer to a reduction in the sampling density of ganglion cell neurons owing to damage to the front-end sensory mechaism, such as loss of RGCs. Also do not be confused with the ratio of RGC to cones or rods.

Methods

Participants

A total of 44 subjects participated in this study: 21 glaucoma patients (mean age ± standard deviation [SD] = 63 ± 8 years), and 23 age-matched older adults with normal or corrected-to-normal vision (mean age = 64 ± 7 years). There was no significant difference in age between the groups (P = 0.59). All participants were recruited from either the University of Alabama at Birmingham (UAB) Callahan Eye Hospital or the UAB campus. All subjects were treated in accordance with the Declaration of Helsinki.

Investigative Ophthalmology & Visual Science

Table. Characteristics for Study Participants

Glaucoma Patient ID	Age (Years)	Sex	MD 24–2(dB)	MD 10–2(dB)	Visual Acuity (logMAR)	Contrast Sensitivity (log Unit)	Pupil Diameter (mm)	Lens Status
S1	62	F	–6.51	–4.60	–0.06	1.65	4.7	NSC 3+
S2	63	M	–2.39	–2.42	0.12	1.65	4.2	IOL
S3	73	M	–23.90	–14.66	0.00	1.20	5.6	IOL
S4	56	M	–27.88	–24.26	0.00	1.40	6.4	NSC 2+
S5	51	M	–2.68	1.06	–0.22	1.75	4.2	NSC 1+
S6	59	F	–1.06	N/A	0.14	1.45	3.3	NSC 2+
S7	61	M	–4.64	–0.36	0.02	1.75	4.7	NSC 1+
S8	61	F	–0.55	0.67	0.04	1.65	N/A	IOL
S9	57	F	–11.31	–0.88	0.18	1.65	5.1	NSC 2+
S10	57	M	–26.74	–14.79	0.16	1.70	4.4	NSC 1+
S11	70	F	–12.38	–20.56	0.08	1.65	4.1	NSC 1+
S12	61	F	–22.45	–8.94	0.02	1.65	5.6	NSC 2+
S13	48	F	–5.34	–1.85	–0.10	1.65	5.3	NSC 1+
S14	69	F	–8.39	–1.57	0.00	1.60	4.8	IOL
S15	59	F	0.16	2.19	–0.18	1.70	6.4	NSC 1+
S16	75	F	–3.08	–4.99	–0.04	1.60	4.1	IOL
S17	66	F	–2.06	–0.96	0.08	1.65	4.3	NSC 2+
S18	76	F	–1.39	–0.65	0.00	1.60	3.9	IOL
S19	74	F	–5.87	–3.06	–0.16	1.60	5.5	IOL
S20	61	F	–13.46	–11.16	–0.16	1.65	3.3	NSC 2+
S21	67	F	–15.22	–10.68	0.12	1.65	7.1	IOL
Mean ± SD	63 ± 8	F:M = 15:6	–9.39 ± 9.05	–6.12 ± 7.57	0.00 ± 0.12	1.61 ± 0.12	4.85 ± 1.02	–
				Normal Controls				
Mean ± SD	64 ± 7	F:M = 12:11	0.51 ± 1.27	0.82 ± 0.94	–0.03 ± 0.07	1.77 ± 0.13	4.37 ± 1.05	–

1+ or 2+, severity of cataracts; F, female; IOL, intraocular lenses; M, male; N/A, not available; NSC, nuclear sclerotic cataracts; SD, standard deviation.

Glaucoma patients included in our study were all diagnosed with primary open-angle glaucoma, confirmed through medical records. These patients met the following three inclusion criteria: (1) glaucomatous optic nerve or nerve fiber layer defect. The presence of the glaucomatous optic nerve was defined by masked review of optic nerve head (ONH) photos by glaucoma specialists using previously published criteria.[56] (2) Glaucomatous visual field defect. This was defined as having a value on Glaucoma Hemifield Test from the Humphrey Field Analyzer outside normal limits. (3) No history of other ocular or neurological diseases or surgeries that may have caused visual field loss.

The visual field test was performed with standard automated perimetry (SAP) using both Swedish interactive testing algorithm (SITA) standard 24-2 and 10-2 tests with a Humphrey Field Analyzer (Carl Zeiss Meditec, Inc., Jena, Germany). The 24-2 test measures 24° temporal and 30° nasal visual field, and the 10-2 test measures 10° temporally and nasally. The pupil diameter of each eye was also obtained from the Humphrey Field Analyzer.

For glaucoma patients, the eye with a lower mean deviation (MD) in 10-2 test was chosen for the experiment only if its visual acuity was better than or equal to 0.2 logMAR (or 20/32 Snellen equivalent). Otherwise, the other eye was chosen. Three out of 21 glaucoma patients were tested on both eyes. The average MD of the tested eyes of glaucoma patients was –9.39 ± 9.05 dB for the 24-2 test, and –6.12 ± 7.57 dB for the 10-2 test. The mean visual acuity (ETDRS [Early Treatment Diabetic Retinopathy Study] charts) and the mean log contrast sensitivity (Pelli-Robson charts) of the tested eyes were 0.00 ± 0.12 logMAR (or 20/20 Snellen equivalent) and 1.61 ± 0.12, respectively.

In the current study, normal vision was defined as best-corrected visual acuity better than or equal to 0.1 logMAR (or 20/25 Snellen equivalent), with no visual field defects in either eye, and without any history of ocular or neurological diseases other than cataracts. The dominant eye (determined by the Miles test) was chosen for the experiment. As summarized in the Table, the average MD of the tested eyes of normal controls was 0.51 ± 1.27 dB for the 24-2 test, and 0.82 ± 0.94 dB for the 10-2 test. The mean visual acuity and the mean log contrast sensitivity were –0.03 ± 0.07 logMAR and 1.77 ± 0.13 respectively.

Measuring Threshold Contrasts Using the Equivalent Input Noise Paradigm

Stimuli. The signal was a sinusoidal grating subtending 1.5° in diameter with a spatial frequency of 1.5 cycles per degree (cpd). The edges of the grating were smoothed with a Gaussian kernel with a standard deviation of 0.2°. The grating was circular in shape, and the mean luminance was 52 cd/m^2. The orientation of the grating was either diagonal-left at a 45° angle or diagonal-right at a 45° angle. The noise image consisted of 21 × 21 independently generated square checks: each noise check (2 × 2 pixels per check subtending approximately 0.07° × 0.07° of visual angle) was generated from a Gaussian distribution with a mean of 0 and a standard deviation (root mean square [RMS] contrast) of either 0 (no noise), 0.02, 0.04, 0.08, 0.16, 0.25, or 0.33. Each noise image was square in shape, subtending 1.5° of the visual field (Fig. 2A). The stimuli were generated and controlled using MATLAB (R2014b; The MathWorks Inc., Natick, MA, USA) and Psychophysics Toolbox extensions[57,58] for Windows 7,

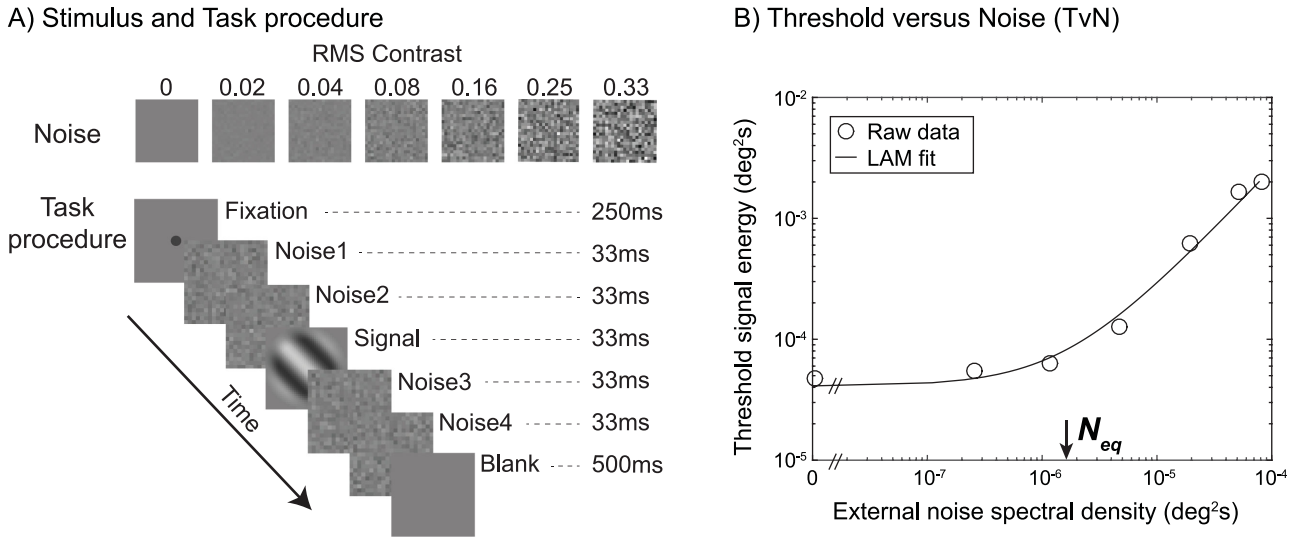

Figure 2. Illustrations of the equivalent input noise paradigm. (**A**) Stimulus and task procedure. *Top*: Noise images. There are seven different noise levels of which the RMS contrast is 0, 0.02, 0.04, 0.08, 0.16, 0.25, and 0.33, respectively. *Bottom*: Task procedure for the orientation discrimination task. (**B**) The threshold versus noise (TvN) curve and model fit. The threshold signal energy (deg^2s) is plotted as a function of external noise spectral density (deg^2s) on log-log coordinates. The *black open dots* represent data points. The *black line* represents the best fit of the LAM to the data. The *arrow* on the horizontal axis represents the equivalent input noise (N_{eq}) derived from the model fit.

running on a PC desktop computer (model: Dell Precision Tower 5810; Dell, Inc., Round Rock, TX, USA). The stimuli were rendered on a 32-in. display++ LCD monitor (Cambridge Research Systems, Ltd., Rochester, UK) with the maximum brightness of 105 cd/m^2. The display had a refresh rate of 120 Hz and a resolution of 1920 × 1080 pixels. All the measurements were made at the viewing distance of 57 cm. The monitor was set to mono++ mode to achieve up to 16-bit grayscale precision. Participants were seated in front of a display monitor in a dark room. A chin-and-head rest was used to minimize head movements while maintaining the constant viewing distance. Stimuli were viewed foveally and monocularly while the nontested eye was covered by an opaque eyepatch.

Task Procedure. A two-alternative forced-choice (2AFC) task was adopted to measure orientation discrimination thresholds. An experimental session was split into a number of blocks. One of the six predetermined noise levels was randomly assigned to each block to eliminate order effects. Each block consisted of 15 trials. At the beginning of each trial, a fixation cross was presented at the center of the screen for 250 ms, immediately followed by a stimulus interval. The stimulus interval was cued with a brief auditory sound. As shown in Figure 2A, the stimulus interval consisted of a signal frame temporally flanked by two noise frames before and after signal. Thus the sequence of the stimulus interval included two consecutive noise frames, a signal frame containing a target grating, and two consecutive noise frames. The duration of each frame was 33 ms. A subject's task was to report the orientation of the grating by pressing either the left or right key. Auditory feedback was given for correct responses. The subject's orientation-discrimination contrast threshold was measured using a 3-down-1-up staircase procedure, which yielded a discrimination accuracy of 79.4%.[59] The step size of the staircase was 2 dB for the first two reversals and then changed to 1 dB for the rest reversals. The staircase for each noise condition was run across a number of blocks until it reached nine reversals. The threshold of each noise condition was determined by taking the geometric mean of the last seven staircase reversals. The subject repeated the session, and the subject's final contrast threshold for each external noise level was taken as the average threshold of the two sessions. The total duration of the experiment was approximately 30 minutes. Prior to the experiment, a practice session was conducted to determine an initial contrast value for a target grating and to help subjects get familiarized with the task procedure.

Data Analyses and Model Fitting. As shown in Figure 2B, the log threshold signal energy was plotted against the log noise power spectral density, and the resulting data were fitted to the linear amplifier model (LAM; see the diagram in Fig. 5)[60,61] as follows:

$$E = \frac{\left(d' + \sqrt{0.5}\right)^2}{J} \times \left(N_{ext} + N_{eq}\right), \quad (1)$$

where E is the threshold signal energy, N_{ext} is the power spectral density of external noise, N_{eq} is the power spectral density of equivalent input noise, J is the calculation efficiency, and d' is the sensitivity index, which is 1.64 at 79.4% accuracy level for a 2AFC task.[59] However, as the phase of the stimulus grating is not fixed in the current study, the sensitivity index can be approximated by $d' + \sqrt{0.5}$.[34,62]

The threshold signal energy E is the integral over space and time of the squared signal contrast:

$$E = t_s \times \int c_s(x,y)^2 dA_s, \quad (2)$$

where $c_s(x,y)$ is the Michelson contrast of a signal pixel at location (x, y), A_s is the area of a signal pixel in deg^2, and t_s is the duration of signal in seconds.

The power spectral density of external noise N_{ext} is the product of the contrast power, area, and duration of a noise

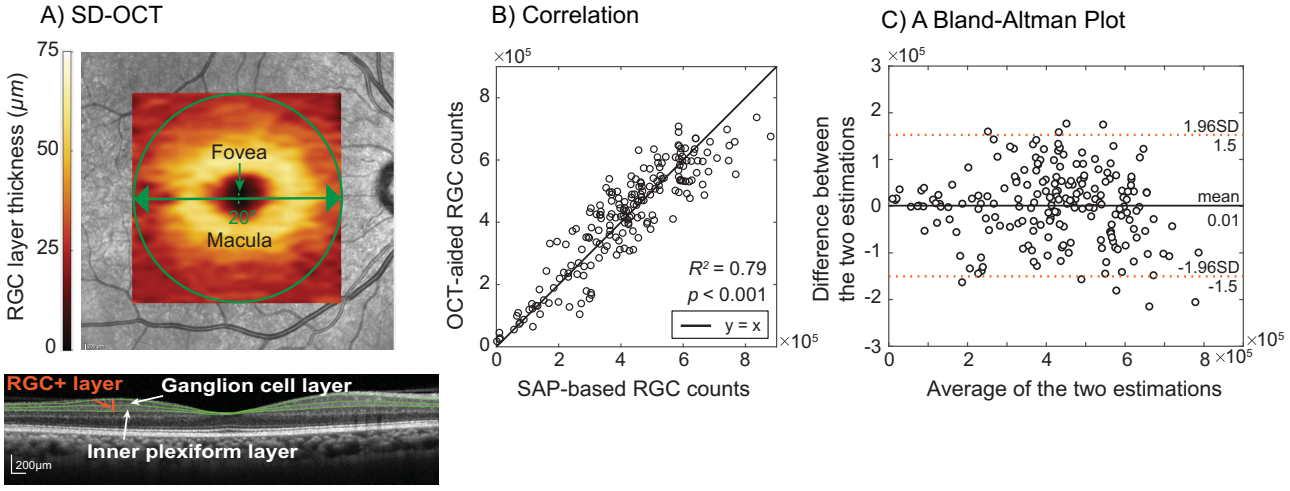

Figure 3. (**A**) Examples of images acquired from SD-OCT. *Top*: An overlay of RGC layer thickness map on a fundus photo. Macular RGC layer thickness map (the heat map) is centered at the fovea. The diameter of the *green circle* corresponds to the central 20° visual field. *Bottom*: A B-scan image, that is a cross-sectional view of the retina. The *green lines* are the boundaries of ganglion cell layer and inner plexiform layer. (**B**) Correlation between estimated macular RGC counts. The OCT-aided RGC counts are pitted against the SAP-based RGC counts. Each *black dot* represents the estimated RGC counts of each subject's tested eye. The *solid line* is the identity line, where $y = x$. (**C**) A Bland-Altman plot. The difference between the two estimations is plotted as a function of the average of the two estimations. Each *black dot* indicates a data point from each subject. The mean difference is the estimated bias of the two estimations indicated by the horizontal *solid black line*. The horizontal *dotted red lines* represent 95% limits of agreement, defined as the mean difference ± 1.96 standard deviation.

check[29,63]:

$$N_{ext} = 4c_n^2 A_n t_n, \quad (3)$$

where 4 indicates the number of noise frames sequentially presented with a signal frame (Fig. 2A), c_n is the RMS contrast of each noise image, A_n is the area of each noise check (2 × 2 pixels) in deg^2, and t_n is the duration of each noise frame in seconds.

The goodness-of-fit of the model was assessed with the R^2 value. The R^2 of the model fits all exceeded 0.8, indicating that the data were well captured by the LAM model.

Measuring the Thickness of Macular RGC+ Layer With Spectral-Domain Optical Coherence Tomography (SD-OCT)

Macular retinal layer thickness was measured with Spectralis SD-OCT (Heidelberg Engineering GmbH, Heidelberg, Germany). The images were generated using high resolution volume scan mode with automatic real-time mean value of 15. Measurements were taken for each subject's tested eye. Macular raster scans were acquired with 49 B-scans consisting of 1024 A-scans. This scan resulted in an imaging area of approximately 6 × 6 mm centered at the fovea, corresponding to the central 20° visual field (Fig. 3A). Any scan with a quality score less than 20 dB was excluded from analysis. The thickness of each layer was read from the automatic segmentation algorithms provided by the onboard SD-OCT software (version 6.3.1.0). The RGC+ layer thickness was the sum of the ganglion cell layer and inner plexiform layer thickness.

Estimating RGC Counts in the Macular Region

For each subject's tested eye the number of RGCs (RGC counts) in the macular region corresponding to the central 20° visual field was estimated based on his or her functional (SAP) and structural (SD-OCT) data. We adopted the estimation methods originally proposed by Harwerth et al.[3,64–66] and Medeiros et al.,[67] with modifications to adjust for the differences in the testing protocol. It should be noted that although previous studies relied on SITA 24-2 test and ONH OCT scans, our study used SITA 10-2 test and macular OCT scans. For this reason, we adjusted for the spacing difference between two adjacent nodes in SITA 10-2 (i.e., 2° apart) and 24-2 (i.e., 6° apart) grids and derived a mathematical function relating the RGC density to age and the severity of visual field defects indicated by MD based on the data collected in our laboratory. We estimated RGC counts in the macular region corresponding to the central 20° visual field. This was done by using all 68 testing locations obtained from the 10-2 visual field (20° × 20°) and the macular OCT image (6 × 6 mm). When we used the macular OCT image corresponding to the central 20° visual field, the degree of the lateral displacement of RGCs becomes negligible, less than 0.5°. For this reason, we did not correct for the lateral displacement for the estimation process. More details of our estimation method can be found in our article in preparation,[68] but in brief, the following steps were taken. Hereafter, the term *SAP-based RGC counts* was used to refer to the estimated RGC counts solely based on SAP data, whereas the term *OCT-aided RGC counts* was used to refer to the estimated RGC counts based on both SAP and OCT data: (1) SAP-based RGC counts. RGC counts were first estimated for each tested eye based on the functional data (SAP sensitivity) and the equations provided in Harwerth et al.[3,65] (2) OCT-aided RGC counts. The RGC density was computed by dividing the RGC counts estimated from the step (1) by the product of the thickness of macular RGC+ layer (SD-OCT) and the corresponding retinal area. RGC+ layer (ganglion cell layer plus inner plexiform layer) was chosen because macular RGC counts were shown to be closely related to the thickness of RGC+ layer ($r^2 = 0.67$, $P < 0.001$).[69] We then incorporated the factors, such as normal aging (age) and the

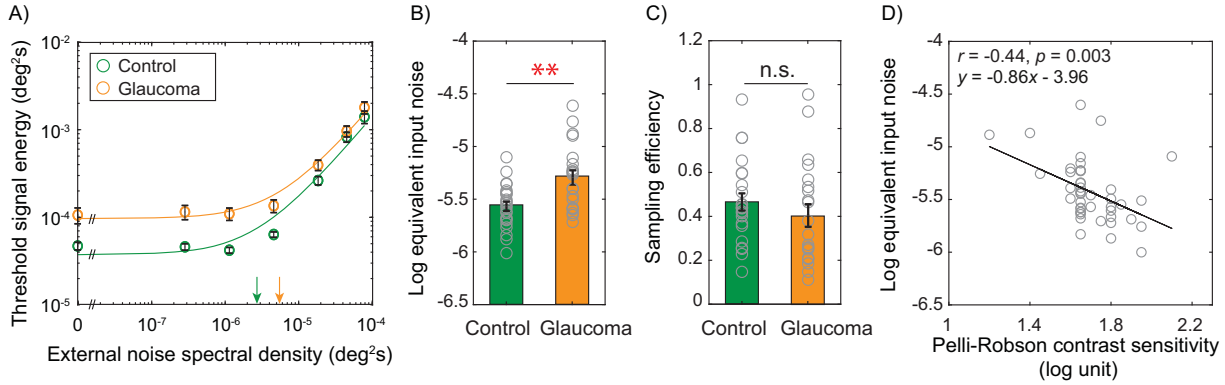

Figure 4. (**A**) Threshold signal energy as a function of external noise spectral density. Each dot represents the mean threshold signal energy of each subject group (*green* for normal vision; *orange* for glaucoma) for a given external noise level. The *solid lines* are the best fit of the LAM to the data. The *arrow* on the horizontal axis represents the equivalent input noise of each subject group. (**B**) Bar graph comparing log equivalent input noise between the groups. (**C**) Bar graph comparing calculation efficiency between the groups. (**D**) Correlations between log equivalent input noise and Pelli-Robson contrast sensitivity. Each *gray dot* represents the data point from each subject. The *solid lines* are the best linear fit to the data. *Error bar* represents ± 1 standard error of the mean. Note that ** indicates $P < 0.01$; n.s. indicates not significant.

severity of visual field defects indicated by MD, into the estimation of the RGC density. This was achieved by integrating two independent linear regression models: one that relates the RGC density to normal aging, and the other that relates the RGC density to MD. The resulting mathematical function enabled us to predict the RGC density from a subject's age and MD. We then estimated RGC counts by computing the product of the subject's macular RGC+ layer thickness, the corresponding retinal area, and the RGC density expected from the subject's age and MD. (3) A weighted sum of the two RGC count estimations. The weighted sum[70] of the SAP-based RGC counts and the OCT-aided RGC counts was computed and adopted as our final estimation of RGC counts for the subject's eye.

For the estimation and validation process, we used the structural and functional data collected from a total of 198 eyes: the right eyes of 67 normally sighted subjects (18–89 years old) and 131 eyes of 77 glaucoma patients (47–89 years old). As shown in Figure 3B, the SAP-based and OCT-aided RGC counts were in an excellent agreement. The majority of the data points were along the identity line, where $y = x$, and 79% of the variance in the OCT-aided RGC counts was explained by the variance in the SAP-based RGC counts ($R^2 = 0.79$, $P < 0.001$). As shown in Figure 3C, the agreement between the two estimations was further evaluated by the Bland-Altman plot,[71,72] in which the difference between two measurements was plotted as a function of the average of the two measurements. The average of the difference (horizontal solid black line) was approximately 1000, indicating that OCT-aided RGC counts were greater than SAP-based RGC counts by 1000 on average. However, the mean difference did not statistically differ from zero ($t_{(197)} = 0.20$, P=0.84), suggesting that there was no systematic bias between the two estimations.

Statistical Analysis

The normality of data was checked with the Shapiro-Wilk Test.[73] The differences between subject groups were compared using the two-tailed independent sample *t*-test, the independent-samples Mann-Whitney *U* test (when the data failed to meet the normality assumption), or the repeated measures analysis of variance (ANOVA). The Pearson correlation and linear regression were also performed to evaluate the relationships between measurements. Statistical analyses were performed using the IBM SPSS statistics version 25 (IBM Corporation, Armonk, NY, USA) in combination with MATLAB R2018a.

Results

A Significant Increase in Equivalent Input Noise in Glaucomatous Central Vision

In Figure 4A, the average threshold signal energy for orientation discrimination for each subject group was plotted as a function of external noise spectral density (TvN curve). As shown by the orange line, glaucoma patients exhibited significantly higher threshold signal energy at the zero noise level (no noise condition) compared with age-matched normally sighted older adults ($t_{(42)} = 4.07$, $P < 0.001$). However, the difference between the two groups became less pronounced with increasing noise spectral density ($F_{(6,252)} = 7.36, P < 0.001$), indicating a noticeable increase in equivalent input noise for glaucomatous vision. Our statistical analysis further confirmed that the log equivalent input noise was significantly higher for glaucoma ($t_{(42)} = 3.45$, $P = 0.001$; Fig. 4B), whereas no significant difference in calculation efficiency was found between the two groups (Mann–Whitney *U* test, $P = 0.27$; Fig. 4C). Furthermore, as shown in Figure 4D, Pelli-Robson contrast sensitivity was significantly correlated with the log equivalent input noise ($r = –0.44, P = 0.003$), but not with the calculation efficiency ($r = 0.27$, $P = 0.08$). These results together suggest that equivalent input noise is significantly elevated in the central vision of glaucoma patients, and the increased equivalent input noise may in part explain foveal contrast sensitivity loss in glaucoma.

Investigative Ophthalmology & Visual Science

Potential Sources of the Increased Equivalent Input Noise in Glaucomatous Central Vision

Then what might have contributed to the observed increase in equivalent input noise in glaucomatous central vision? Here we investigated potential sources of the increased equivalent input noise in glaucomatous central vision: whether it is largely due to optical and/or neural factors.

Optical Factors, Such as Pupil Size and Lens Opacity. It is well-documented that normal aging[74,75] or ocular pathologies, such as glaucoma,[76] alter optical properties, such as pupil size and lens opacity. These properties have been shown to affect equivalent input noise.[61,77,78] Thus here we examined whether any difference in pupil size and/or lens opacity between normal and glaucoma groups might have resulted in the observed difference in equivalent input noise between the two groups.

First, the effect of pupil size was assessed by comparing the average pupil size between glaucoma and normal controls and performing the correlation between pupil size and equivalent input noise across subjects. We, however, did not find any significant difference in pupil diameter (P = 0.13) between the two groups nor any significant correlation between pupil diameter and log equivalent input noise (P = 0.17). Second, the effect of lens opacity, that is, cataracts, was evaluated by performing two separate analyses: (1) glaucoma patients were divided into two subgroups: ones with cataracts (n = 13) and ones without cataracts (n = 8), and the difference in equivalent input noise between the two subgroups was compared. However, there was no significant difference between the two groups (P = 0.76). (2) We compared equivalent input noise between the two eyes of glaucoma patients who exhibited a great deal of binocularly asymmetric glaucomatous damage (i.e., interocular difference of 10-2 MD larger than 8 dB). Despite comparable optical quality between the two eyes of these patients (n = 3), the eye with severer glaucoma consistently exhibited a larger equivalent input noise compared with the fellow eye (7.30 vs. 4.07 $\mu deg^2 s$). On average, the increase of equivalent input noise in the worse eye was 81%, which was much greater than the difference of calculation efficiency (18%). Taken together, our results suggest that neither pupil size nor lens opacity alone is likely to explain the increased equivalent input noise observed in our glaucoma group.

Retinal Undersampling Due to Ganglion Cell Damage. RGC damage may elevate neural noise due to associated neuronal dysfunction in the retina or/and the cortex, but also may reduce spatial sampling at the retinal level (i.e., a reduction in the RGC density). Equivalent input noise is often viewed as internal noise in the visual system, whereas calculation efficiency (also termed as sampling efficiency[79]) is known to represent the efficiency with which the human observer samples the available information relative to an ideal observer. For this reason, undersampling due to neuronal loss (e.g., a loss of RGCs) has been associated with a reduction in calculation efficiency.[52,80,81] However, here we demonstrated that retinal undersampling resulting from ganglion cell damage may predominantly affect equivalent input noise. To evaluate the effect of retinal undersampling, we incorporated an RGC sampling module into the LAM. As illustrated in the top panel of Figure 5, in the LAM, the human visual system is assumed to consist of additive internal noise and the calculation that transforms the stimulus (i.e., signal plus external noise) and internal noise into a decision variable. Now we introduce the undersampling at the retinal level to mimic a loss of RGCs in glaucomatous eyes. We first partitioned internal noise into two stages: the early stage of internal noise (N_{eq1}) arising from optical properties, and the late stage of internal noise (N_{eq2}) resulting from neuronal properties. The RGC sampling module was then inserted between the two stages of internal noise (the bottom panel of Fig. 5). Let us denote the resulting effect of RGC sampling on signal as $s_1$and its resulting effect on either external noise (N_{ext}) or the early internal noise (N_{eq1}) as s_2. Then we can express Equation 1 as follows:

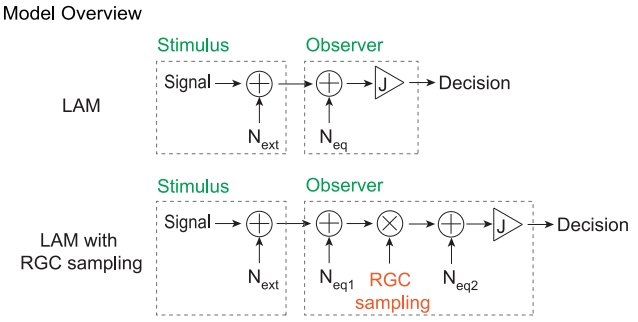

Figure 5. Schematic diagrams of the LAM and the modified LAM with the module of sampling at the retina (i.e., RGC sampling). *Top*: The original LAM. In the LAM, the human visual system is assumed to consist of an additive internal noise (N_{eq}) and a calculation (its efficiency is J) transforming the stimulus (i.e., a signal plus external noise N_{ext}) and N_{eq} to a decision. *Bottom*: The modified LAM. In this model, the source of the equivalent input noise (N_{eq}) is divided into two: the early noise (N_{eq1}) and the late noise (N_{eq2}). The module of RGC sampling is then added between the two noise sources.

$$s_1 E = \frac{\left(d' + \sqrt{0.5}\right)^2}{J} \times \left(s_2 N_{ext} + s_2 N_{eq1} + N_{eq2}\right), \qquad (4)$$

which is equal to

$$E = \frac{\left(d' + \sqrt{0.5}\right)^2}{\left(\frac{s_1}{s_2}\right) J} \times \left(N_{ext} + N_{eq1} + \frac{N_{eq2}}{s_2}\right). \qquad (5)$$

When we let $N_{eq}{}' = N_{eq1} + \frac{N_{eq2}}{s_2}$ and $J' = (\frac{s_1}{s_2})J$, we can express Equation 5 in the form of Equation 1 as follows:

$$E = \frac{\left(d' + \sqrt{0.5}\right)^2}{J'} \times \left(N_{ext} + N_{eq}{}'\right), \qquad (6)$$

where $N_{eq}{}'$ represents the sum of the early internal noise and the late internal noise scaled by s_2, and J' represents the calculation efficiency scaled by $\frac{s_1}{s_2}$, the relative effect of RGC sampling on signal and external noise.

Hence when $s_1 = s_2$, $J' = (\frac{s_1}{s_2})J = J$.

Therefore when the effect of RGC sampling on signal and external noise is assumed to be equal, the calculation efficiency J would remain unchanged even with changes in the sampling of the retina image. In other words, our mathematical derivation demonstrates that the equivalent input noise can be expressed as a function of internal noise and the effect of retinal sampling (i.e., $N_{eq}{}' = N_{eq1} + \frac{N_{eq2}}{s_2}$) in the linear system.

Our analytical derivation relies on the assumption that signal (s_1) and external noise (s_2) are equally affected by

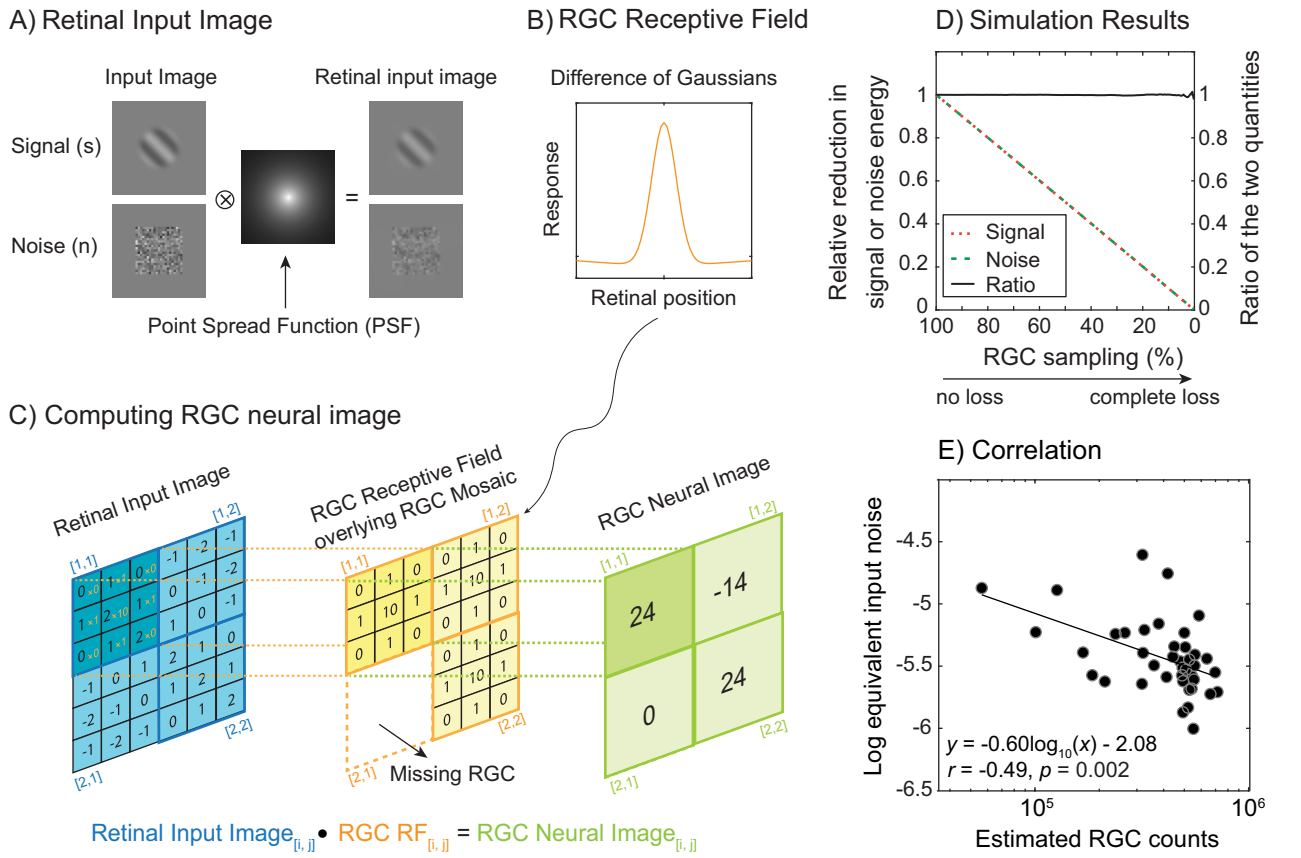

Figure 6. (**A**) Retinal input image. Retinal input image was computed by convolving an input image (i.e., signal or noise) with the point spread function of the human eye. (**B**) RGC receptive field. The RGC receptive field was modeled by a difference of 2D Gaussians. (**C**) Computing RGC neural image. RGC neural image is the RGC responses to a given retinal input image. The RGC response for a given grid was estimated as the dot product of the retinal input image centered at the grid [*i*,*j*] and the corresponding RGC receptive field. Each square with *orange frame* denotes the receptive field size of an RGC (for illustration purpose, only center receptive fields of RGCs are shown here), whereas squares with *dark blue* and *green frame* denote the RGC corresponding retinal input image and RGC response. The *dashed orange square* represents a missing RGC unit in the retina. For computational simplicity, the neuronal response to the blank background (i.e., the mean luminance of signal and noise) was used to fill in the missing part of the neural image. Note that the numbers shown in cells and squares are arbitrary. (**D**) Simulation results. The relative reduction in the energy of signal or noise caused by random RGC undersampling with respect to the energy at 100% RGC sampling is plotted for varying degrees of RGC sampling. The *y*-axis on the left shows the relative reduction in signal (*orange dotted line*) and noise (*green dashed line*) energy. The *y*-axis on the right indicates the ratio of the two quantities (*black solid line*). (**E**) Correlation between log equivalent input noise and the estimated RGC counts across subjects.

RGC sampling. This simple assumption was adopted based on the principle of Occam's razor, but we also proved the assumption using a simple retinal model[82–84] mimicking a loss of RGCs. Here are a brief overview of our model and the results of the model simulation.

The effects of RGC loss on signal and noise were simulated by computing RGC responses (hereafter RGC neural image or neural image) to a given retinal input image. The simulation had three main components:

(1) Retinal input image. Retinal input image contained either signal, noise, or background image. The signal and noise stimulus were identical to the ones used in our psychophysical experiment (see the Methods). As shown in Figure 6A, retinal input image was computed by convolving the stimulus (signal or noise) or background image (a blank background with the mean luminance of signal and noise) with the point spread function of the human eye[85] as follows:

$$Retinal\ Input\ Image_{s,n,or\,b} = PSF \otimes I, \quad (7)$$

where *PSF* is the point spread function of the eye, and *I* is the input image of either signal (*s*), noise (*n*), or background (*b*).

(2) RGC mosaic and receptive field. Let $RGC_{[i,j]}$ denote the RGC at row *i*, column *j* on the RGC mosaic (i.e., a grid). A loss of RGCs was simulated by randomly removing a certain amount of RGCs from the mosaic that led to random undersampling. As shown in Figure 6B, RGC receptive field was modeled by a difference of two-dimensional (2D) Gaussians.[26,86] The RGC receptive field centered at each grid was computed as follows:

$$RGC\ Receptive\ Field_{[i,j]} = k_c \times \exp\left(-\left(\frac{d}{r_c}\right)^2\right) - k_s \times \exp\left(-\left(\frac{d}{r_s}\right)^2\right), \quad (8)$$

where k_c is the peak sensitivity of center receptive field, r_c is the radius of center receptive field size, k_s is the peak

sensitivity of surround receptive field, r_s is the radius of surround receptive field size, and d is the Euclidean distance between a retinal location (x, y) and the center of $RGC_{[i,j]}$. As midget RGCs make up to 80–90% ganglion cells in the foveal region,[87,88] we used the receptive field parameters of midget RGCs at retinal eccentricities ranging from 0° to 5°.[86]

(3) RGC neural image. As shown in Figure 6C, the RGC response for a given grid [*i,j*] was computed as a dot product of the retinal input image centered at the grid and the corresponding RGC receptive field.

$$Neural\ Image_{[i,j]} = Retinal\ Input\ Image_{[i,j]} \cdot RGC\ Receptive\ Field_{[i,j]}. \quad (9)$$

Note that for illustration purpose, only the center receptive fields of RGCs are shown in Figure 6C.

When there is a loss of RGC in the retina, a part of the retinal input image falling onto the missing part of the RGC mosaic does not invoke any neural responses. In our model simulation, a neural response to the blank background (i.e., the mean luminance of signal and noise) was used to fill in the missing part of neural image as shown in Figure 6C. This was done for computational simplicity. We simulated varying degrees of RGC sampling ranging from 100% (no RGC loss) to 0% (a complete loss of RGCs) and obtained corresponding neural images. Each simulation run was based on multiple times of random undersampling of the RGC mosaic as described earlier. We repeated the simulation 1000 times, and the final result was the average of the 1000 simulations. For a given neural image, the energy of signal or noise was computed using Equations 2 or 3, and then the amount of the reduction in the energy following RGC undersampling relative to the energy at 100% RGC sampling was computed.

To evaluate whether RGC random undersampling impacts signal and noise equally, we compared the amount of the reduction in the energy of signal and that of noise. As shown in Figure 6D, the energy of signal (orange dotted line) and the energy of noise (green dashed line) linearly decreases with decreasing RGC sampling at the same rate, that was further confirmed by the ratio of the two quantities (black solid line) remaining constant at 1 across varying degrees of RGC sampling. These results appear to support the assumption of our model: the effect of RGC loss on signal and noise are likely to be equal.

It should be noted that although the RGC receptive field function was fixed for the foregoing simulation, the pattern of the simulation results remained the same even when different RGC receptive field functions, such as receptive fields of parasol ganglion cells or RGC receptive fields at different eccentricities, were applied.

To confirm the prediction made from our foregoing analytical derivation, that is, RGC sampling may predominantly affect equivalent input noise but not calculation efficiency, we further examined the relationship between the equivalent input noise (or calculation efficiency) and the macular RGC counts of the tested eye across subjects. The number of RGCs for each subject's tested eye was estimated based on the structural (SD-OCT) and functional (SAP) data (see the Methods for details) of the tested eye. As shown in Figure 6E, we found that the log equivalent input noise was significantly correlated with the estimated number of RGCs (r = –0.49, P = 0.002), but not with calculation efficiency (P = 0.59). Furthermore, our regression analysis showed that approximately 24% of variance in equivalent input noise can be accounted for by the macular RGC counts (R^2 = 0.24, P = 0.001). Consistent with these results, the log equivalent input noise was also significantly correlated with the thickness of macular RGC+ layer (r = –0.41, P = 0.006). Thus our empirical results are in good agreement with our analytical prediction that retinal undersampling likely affects equivalent input noise.

Our empirical results together with analytical derivation and model simulation convinced us to believe that the retinal undersampling following RGC damage might have played a role in the increased equivalent input noise in the central vision of glaucoma.

Discussion

In this study, we investigated the mechanism underpinning contrast sensitivity loss in the central vision of glaucoma patients. To address this question, the classical equivalent input noise paradigm[61,63,89] was adopted. Our results showed that compared with age-matched normal vision, glaucomatous vision exhibited a significant increase in equivalent input noise. Yet, no significant difference was found for calculation efficiency. Using analytical derivation, empirical data analyses, and model simulation, we further demonstrated that the increased equivalent input noise in the central vision appeared to be related to retinal undersampling following RGC damage. Of course, we cannot rule out a potential role of calculation efficiency in glaucomatous contrast sensitivity deficits given the relatively small sample size (n = 21 for glaucoma patients). However, the difference in equivalent input noise (~120%) between normal and glaucomatous vision was substantially larger than the difference observed in efficiency (~13%). Furthermore, we observed a significant correlation between foveal contrast sensitivity and equivalent input noise, but not efficiency. Thus the current study further investigated potential sources of increased equivalent input noise in glaucomatous vision.

Changes in the optical properties, such as optical defocus, pupil miosis, or cataract, are known to affect equivalent input noise but not calculation efficiency[61,77,78,90] (but also see Liang et al.[91]). However, these optical properties alone do not appear to explain the increased equivalent input noise observed in our glaucoma patients. In the current study, optical aberrations, such as defocus and astigmatism, were relatively well controlled as our experiment was conducted with a subject's best-corrected visual acuity at the viewing distance. There was no significant difference in either the best-corrected visual acuity (P = 0.24) or pupil diameter (P = 0.13) between glaucoma patients and normal controls. In addition, the effect of cataracts on our results was rather negligible, consistent with previous studies showing that the optical properties, such as nuclear cataracts[92–94] and uncorrected higher-order aberrations,[91,95,96] have no or little effect on contrast sensitivity at relatively low spatial frequencies, including the spatial frquency of 1.5 cpd used in our study. Although we do not dismiss the known effect of the optical properties on equivalent input noise in general, the results from our analysis suggest that these optical properties alone were not likely to give rise to the increased equivalent input noise observed in glaucoma patients.

On the other hand, our results showed that the increased equivalent input noise in glaucoma might be in part ascribed to retinal undersampling. A study done by McAnany and

Investigative Ophthalmology & Visual Science

Park[49] also showed that an increase in equivalent input noise is associated with contrast sensitivity loss in diabetic patients, and a significant loss of RGCs was also reported in diabetic patients.[97] Pelli et al.[98,99] also showed that the equivalent input noise, not calculation efficiency, increases with increasing retinal eccentricities. Note that the sampling density of neurons decreases and the receptive field size increases with increasing eccentricity. Thus we can speculate that even if the loss of RGCs is fully compensated by an enlargement of receptive fields at either retinal or cortical level, equivalent input noise may still increase with loss of RGCs as what has been observed in normal peripheral vision. Furthermore, Baldwin et al.[31] pointed out that changes in sampling (e.g., reduced neuronal density) can be manifested as changes in equivalent input noise when the linear assumption of the LAM is violated, again suggesting a potential effect of retinal undersampling on equivalent input noise. We, however, cannot rule out the fact that increased neural noise due to structural and functional abnormalities in the retina or/and the cortex following RGC damage might have contributed to the increased equivalent input noise. Previous studies on animal models of glaucoma indeed reported that, preceding the death of ganglion cells, abnormalities arise in the structure and function of ganglion cells, that include dysfunction and degeneration of axons, reduction in dendritic fields, and changes in soma size.[100–102] Furthermore, brain imaging studies have reported structural, functional, and metabolic abnormalities in glaucomatous brains,[103–105] such as abnormal spontaneous activities in visual and other cortical areas of the brain.[106,107]

In our study, the RGC counts were estimated based on a combination of SAP and SD-OCT data. This combined estimation appeared to be as a better index for staging and detecting glaucomatous damage compared with each separate estimation.[67] The original equations used for the combined estimation have been verified by monkey and human histological data.[3,65] However, we acknowledge the weaknesses of the combined method reported in previous studies. For example, it has been shown that the OCT-aided RGC counts are consistently lower than the SAP-based RGC counts.[108,109] This issue may become less relevant to our estimation because our OCT-aided estimation relied on macular OCT scans of the RGC+ layer instead of ONH OCT scans used in previous studies. On the other hand, Raza and Hood[110] reported that SAP-based RGC counts appeared to be much larger than expected from some of the histological studies.[2,111] It is still unclear what might have caused this apparent discrepancy. Although speculated, it may be in part because of the relatively small samples used in histological studies (e.g., n = 6),[111] an indirect estimation of RGC counts from the number of RGC nerve fibers around the ONH,[2] and/or the interindividual variability in the number of RGCs.

We also acknowledge that there was a noticeable mismatch between the area where RGC counts were estimated and where the equivalent input noise was measured psychophysically: RGC counts were estimated in the macular region corresponding to the central 20° visual field, whereas our psychophysical target stimulus centered at the fovea was 1.5° in diameter. Although it is ideal to obtain RGC counts in the retinal region underlying the target stimulus, identifying the precise retinal region involved in processing a relatively small foveal stimulus is challenging. It is because the degree of the lateral displacement of RGC bodies becomes substantial (up to 3°–4° displacement) at the foveal region, and there is also large intersubject variability in retinal structure.[111] For these reasons, we went on to further confirm whether the pattern of our results still holds true for the foveal region narrowly encompassing the target location. We estimated the RGC counts in the retinal region corresponding to the central 4° visual field based on the SAP data only. The procedure was identical to the step (1) in the Methods, except that only central four data points in SITA 10-2 test were used. We found that the correlation between equivalent input noise and RGC counts remains statistically significant ($r = -0.51$, $P < 0.001$) even in the narrowly defined foveal region.

Conclusions

Using the equivalent input noise paradigm, we showed that contrast sensitivity loss in the central vision of glaucoma patients is largely accounted for by an increase in equivalent input noise. Furthermore, our findings showed that the increased equivalent input noise may in part be due to retinal undersampling in glaucomatous vision, highlighting the impact of RGC damage on the central pattern vision of glaucoma. To our knowledge, this is the first report demonstrating how the sampling property at the retinal level may impact the system's equivalent input noise.

Acknowledgments

The authors thank Lindsay Washington and Victoria Chen for proofreading.

Supported by the National Institutes of Health/National Eye Institute Grant R01EY027857, Research to Prevent Blindness (RPB)/Lions Clubs International Foundation (LCIF) low vision research award, and the EyeSight Foundation of Alabama (MK). The sponsor or funding organization had no role in the design or conduct of this research. The authors alone are responsible for the content and writing of the article.

A part of this material was presented at the Annual Meeting of the Association for Research in Vision and Ophthalmology (ARVO), 2018.

Disclosure: **R. Liu**, None; **M. Kwon**, None

References

1. Quigley HA. Neuronal death in glaucoma. *Prog Retin Eye Res*. 1999;18:39–57.
2. Kerrigan–Baumrind LA, Quigley HA, Pease ME, Kerrigan DF, Mitchell RS. Number of ganglion cells in glaucoma eyes compared with threshold visual field tests in the same persons. *Invest Ophthalmol Vis Sci*. 2000;41:741–748.
3. Harwerth RS, Carter-Dawson L, Smith EL 3rd, Barnes G, Holt WF, Crawford ML. Neural losses correlated with visual losses in clinical perimetry. *Invest Ophthalmol Vis Sci*. 2004;45:3152–3160.
4. Tan O, Chopra V, Lu AT, et al. Detection of macular ganglion cell loss in glaucoma by Fourier-domain optical coherence tomography. *Ophthalmology*. 2009;116:2305–2314.e2301-2302.
5. Hood DC, Raza AS, de Moraes CG, Liebmann JM, Ritch R. Glaucomatous damage of the macula. *Prog Retin Eye Res*. 2013;32:1–21.
6. Kwon M, Liu R. Linkage between retinal ganglion cell density and the nonuniform spatial integration across the visual field. *Proc Natl Acad Sci U S A*. 2019;116:3827–3836.

7. Ramulu PY, S KW, Munoz B, Jampel HD, Friedman DS. Glaucoma and reading speed. *Arch Ophthalmol*. 2009;127:82–87.
8. Ramulu P. Glaucoma and disability: which tasks are affected, and at what stage of disease? *Curr Opin Ophthalmol*. 2009;20:92–98.
9. Glen FC, Smith ND, Crabb DP. Saccadic eye movements and face recognition performance in patients with central glaucomatous visual field defects. *Vision Res*. 2013;82:42–51.
10. Kwon M, Liu R, Patel BN, Girkin C. Slow reading in glaucoma: is it due to the shrinking visual span in central vision? *Invest Ophthalmol Vis Sci*. 2017;58:5810–5818.
11. Burton R, Crabb DP, Smith ND, Glen FC, Garway-Heath DF. Glaucoma and reading: exploring the effects of contrast lowering of text. *Optom Vis Sci*. 2012;89:1282–1287.
12. Onal S, Yenice O, Cakir S, Temel A. FACT contrast sensitivity as a diagnostic tool in glaucoma: FACT contrast sensitivity in glaucoma. *Int Ophthalmol*. 2008;28:407–412.
13. Kara S, Gencer B, Ersan I, et al. Repeatability of contrast sensitivity testing in patients with age-related macular degeneration, glaucoma, and cataract. *Arq Bras Oftalmol*. 2016;79.
14. Chien L, Liu R, Girkin C, Kwon M. Higher contrast requirement for letter recognition and macular RGC+ layer thinning in glaucoma patients and older adults. *Invest Ophthalmol Vis Sci*. 2017;58:6221–6231.
15. Ansari EA, Morgan JE, Snowden RJ. Psychophysical characterisation of early functional loss in glaucoma and ocular hypertension. *Br J Ophthalmol*. 2002;86:1131–1135.
16. Hawkins AS, Szlyk JP, Ardickas Z, Alexander KR, Wilensky JT. Comparison of contrast sensitivity, visual acuity, and Humphrey visual field testing in patients with glaucoma. *J Glaucoma*. 2003;12:134–138.
17. Leat SJ, Woo GC. The validity of current clinical tests of contrast sensitivity and their ability to predict reading speed in low vision. *Eye (Lond)*. 1997;11:893–899.
18. Legge GE, Rubin GS, Luebker A. Psychophysics of reading—V. The role of contrast in normal vision. *Vision Res*. 1987;27:1165–1177.
19. Moes E, Lombardi KM. The relationship between contrast sensitivity, gait, and reading speed in Parkinson's disease. *Neuropsychol Dev Cogn B Aging Neuropsychol Cogn*. 2009;16:121–132.
20. Owsley C, Sloane ME. Contrast sensitivity, acuity, and the perception of "real-world" targets. *Br J Ophthalmol*. 1987;71:791–796.
21. Kwon M, Legge GE. Higher-contrast requirements for recognizing low-pass-filtered letters. *J Vis*. 2013;13:13–13.
22. Duggan E, et al. Time to refocus assessment of vision in older adults? Contrast sensitivity but not visual acuity is associated with gait in older adults. *J Gerontol A Biol Sci Med Sci*. 2017;72:1663–1668.
23. Owsley C, Stalvey BT, Wells J, Sloane ME, McGwin G, Jr. Visual risk factors for crash involvement in older drivers with cataract. *Arch Ophthalmol*. 2001;119:881–887.
24. Kwon M, Huisingh C, Rhodes LA, McGwin G, Jr., Wood JM, Owsley C. Association between Glaucoma and At-fault Motor Vehicle Collision Involvement among Older Drivers: A Population-based Study. *Ophthalmology*. 2016;123:109–116.
25. Owsley C. Contrast sensitivity. *Ophthalmol Clin North Am*. 2003;16:171–177.
26. Enroth-Cugell C, Robson JG. The contrast sensitivity of retinal ganglion cells of the cat. *J Physiol*. 1966;187:517–552.
27. Raghavan M. *Sources of Visual Noise. [Doctor of Philosophy (PhD) thesis]*. Syracuse, NY: Syracuse University; 1995.
28. Allard R, Faubert J, Pelli DG. Editorial: using noise to characterize vision. *Front Psychol*. 2015;6:1707.
29. Pelli DG, Farell B. Why use noise? *J Opt Soc Am A Opt Image Sci Vis*. 1999;16:647–653.
30. Hayes RD, Merigan WH. Mechanisms of sensitivity loss due to visual cortex lesions in humans and macaques. *Cereb Cortex*. 2007;17:1117–1128.
31. Baldwin AS, Baker DH, Hess RF. What do contrast threshold equivalent noise studies actually measure? Noise vs. nonlinearity in different masking paradigms. *PLoS One*. 2016;11:e0150942.
32. Dakin SC, Mareschal I, Bex PJ. Local and global limitations on direction integration assessed using equivalent noise analysis. *Vision Res*. 2005;45:3027–3049.
33. Betts LR, Sekuler AB, Bennett PJ. The effects of aging on orientation discrimination. *Vision Res*. 2007;47:1769–1780.
34. Bennett PJ, Sekuler AB, Ozin L. Effects of aging on calculation efficiency and equivalent noise. *J Opt Soc Am A Opt Image Sci Vis*. 1999;16:654–668.
35. Pardhan S, Gilchrist J, Elliott DB, Beh GK. A comparison of sampling efficiency and internal noise level in young and old subjects. *Vision Res*. 1996;36:1641–1648.
36. Allard R, Renaud J, Molinatti S, Faubert J. Contrast sensitivity, healthy aging and noise. *Vision Res*. 2013;92:47–52.
37. Pardhan S. Contrast sensitivity loss with aging: sampling efficiency and equivalent noise at different spatial frequencies. *J Opt Soc Am A Opt Image Sci Vis*. 2004;21:169–175.
38. Lu ZL, Dosher BA. Perceptual learning retunes the perceptual template in foveal orientation identification. *J Vis*. 2004;4(1):5.
39. Chung ST, Levi DM, Tjan BS. Learning letter identification in peripheral vision. *Vision Res*. 2005;45:1399–1412.
40. Gold J, Bennett PJ, Sekuler AB. Signal but not noise changes with perceptual learning. *Nature*. 1999;402:176–178.
41. Lu Z-L, Dosher BA. External noise distinguishes attention mechanisms. *Vision Res*. 1998;38:1183–1198.
42. Hou F, Lu ZL, Huang CB. The external noise normalized gain profile of spatial vision. *J Vis*. 2014;14(13):9.
43. Silvestre D, Arleo A, Allard R. Internal noise sources limiting contrast sensitivity. *Sci Rep*. 2018;8:2596.
44. Chen G, Hou F, Yan F-F, et al. Noise Provides New Insights on Contrast Sensitivity Function. *PLoS One*. 2014;9:e90579.
45. Xu P, Lu ZL, Qiu Z, Zhou Y. Identify mechanisms of amblyopia in Gabor orientation identification with external noise. *Vision Res*. 2006;46:3748–3760.
46. Levi DM, Klein SA, Chen I. What limits performance in the amblyopic visual system: seeing signals in noise with an amblyopic brain. *J Vis*. 2008;8(4):1.
47. Huang C, Tao L, Zhou Y, Lu Z-L. Treated amblyopes remain deficient in spatial vision: a contrast sensitivity and external noise study. *Vision Res*. 2007;47:22–34.
48. McAnany JJ, Alexander KR, Genead MA, Fishman GA. Equivalent intrinsic noise, sampling efficiency, and contrast sensitivity in patients with retinitis pigmentosa. *Invest Ophthalmol Vis Sci*. 2013;54:3857–3862.
49. McAnany JJ, Park JC. Reduced contrast sensitivity is associated with elevated equivalent intrinsic noise in type 2 diabetics who have mild or no retinopathy. *Invest Ophthalmol Vis Sci*. 2018;59:2652–2658.
50. Christensen BK, Spencer JM, King JP, Sekuler AB, Bennett PJ. Noise as a mechanism of anomalous face processing among persons with schizophrenia. *Front Psychol*. 2013;4:401.
51. Sperling AJ, Lu ZL, Manis FR, Seidenberg MS. Deficits in perceptual noise exclusion in developmental dyslexia. *Nat Neurosci*. 2005;8:862–863.

Investigative Ophthalmology & Visual Science

52. Falkenberg HK, Bex PJ. Sources of motion-sensitivity loss in glaucoma. *Invest Ophthalmol Vis Sci*. 2007;48:2913–2921.
53. Wassle H, Riemann HJ. The mosaic of nerve cells in the mammalian retina. *Proc R Soc Lond B Biol Sci*. 1978;200:441–461.
54. Dacey DM. Physiology, morphology and spatial densities of identified ganglion cell types in primate retina. *Ciba Found Symp*. 1994;184:12–28; discussion 28–34, 63–70.
55. Hofer H, Carroll J, Neitz J, Neitz M, Williams DR. Organization of the human trichromatic cone mosaic. *J Neurosci*. 2005;25:9669–9679.
56. Sample PA, Girkin CA, Zangwill LM, et al. The African Descent and Glaucoma Evaluation Study (ADAGES): design and baseline data. *Arch Ophthalmol*. 2009;127:1136–1145.
57. Brainard DH. The Psychophysics Toolbox. *Spat Vis*. 1997;10:433–436.
58. Pelli DG. The VideoToolbox software for visual psychophysics: transforming numbers into movies. *Spat Vis*. 1997;10:437–442.
59. Wetherill GB, Levitt H. Sequential estimation of points on a psychometric function. *Br J Math Stat Psychol*. 1965;18:1–10.
60. Pelli DG. *Effects of Visual Noise [doctoral dissertation]*. Cambridge, England: Cambridge University; 1981.
61. Pelli DG. The quantum efficiency of vision. In: Blakemore C (ed), *Vision: Coding and Efficiency*. Cambridge: Cambridge University Press; 1990:3–24.
62. Jeffress LA. Stimulus-oriented approach to detection. *J Acoust Soc Am*. 1964;36:766–774.
63. Legge GE, Kersten D, Burgess AE. Contrast discrimination in noise. *J Opt Soc Am A*. 1987;4:391–404.
64. Harwerth RS, Wheat JL, Fredette MJ, Anderson DR. Linking structure and function in glaucoma. *Prog Retin Eye Res*. 2010;29:249–271.
65. Harwerth RS, Quigley HA. Visual field defects and retinal ganglion cell losses in patients with glaucoma. *Arch Ophthalmol*. 2006;124:853–859.
66. Harwerth RS, Wheat JL, Rangaswamy NV. Age-related losses of retinal ganglion cells and axons. *Invest Ophthalmol Vis Sci*. 2008;49:4437–4443.
67. Medeiros FA, Lisboa R, Weinreb RN, Girkin CA, Liebmann JM, Zangwill LM. A combined index of structure and function for staging glaucomatous damage. *Arch Ophthalmol*. 2012;130:1107–1116.
68. Kwon M, Liu R. (May 2020). *Structural and functional changes associated with varying degrees of retinal ganglion cell loss*. Vision Sciences Society (VSS), St. Pete Beach, FL, USA.
69. Zhang C, Tatham AJ, Weinreb RN, et al. Relationship between ganglion cell layer thickness and estimated retinal ganglion cell counts in the glaucomatous macula. *Ophthalmology*. 2014;121:2371–2379.
70. Medeiros FA, Zangwill LM, Bowd C, Mansouri K, Weinreb RN. The structure and function relationship in glaucoma: implications for detection of progression and measurement of rates of change. *Invest Ophthalmol Vis Sci*. 2012;53:6939–6946.
71. Altman DG, Bland JM. Measurement in medicine: the analysis of method comparison studies. *Statistician*. 1983;32:307–317.
72. Bland JM, Altman D. Statistical methods for assessing agreement between two methods of clinical measurement. *Lancet*. 1986;327:307–310.
73. Shapiro SS, Wilk MB. An analysis of variance test for normality (complete samples)†. *Biometrika*. 1965;52:591–611.
74. Birren JE, Casperson RC, Botwinick J. Age changes in pupil size. *J Gerontol*. 1950;5:216–221.
75. Klein BE, Klein R, Linton KL. Prevalence of age-related lens opacities in a population. The Beaver Dam Eye Study. *Ophthalmology*. 1992;99:546–552.
76. Park JW, Kang BH, Kwon JW, Cho KJ. Analysis of various factors affecting pupil size in patients with glaucoma. *BMC Ophthalmology*. 2017;17:168.
77. Pardhan S, Gilchrist J, Beh GK. Contrast detection in noise: a new method for assessing the visual function in cataract. *Optom Vis Sci*. 1993;70:914–922.
78. Kersten D, Hess RF, Plant GT. Assessing contrast sensitivity behind cloudy media. *Clin Vis Sci*. 1988;2:143–158.
79. Burgess AE, Wagner RF, Jennings RJ, Barlow HB. Efficiency of human visual signal discrimination. *Science*. 1981;214:93.
80. Bogfjellmo LG, Bex PJ, Falkenberg HK. Reduction in direction discrimination with age and slow speed is due to both increased internal noise and reduced sampling efficiency. *Invest Ophthalmol Vis Sci*. 2013;54:5204–5210.
81. Yates JT, Leys MJ, Green M, et al. Parallel pathways, noise masking and glaucoma detection: behavioral and electrophysiological measures. *Doc Ophthalmol*. 1998;95:283–299.
82. Thibos LN. Chapter 1 – Formation and Sampling of the Retinal Image. In: De Valois KK (ed), *Seeing*. San Diego: Academic Press; 2000:1–54.
83. Bradley C, Abrams J, Geisler WS. Retina-V1 model of detectability across the visual field. *J Vis*. 2014;14(12):22.
84. Watson AB, Ahumada AJ. Letter identification and the Neural Image Classifier. *J Vis*. 2015;15(2):15.
85. Navarro R, Artal P, Williams DR. Modulation transfer of the human eye as a function of retinal eccentricity. *J Opt Soc Am A*. 1993;10:201–212.
86. Croner LJ, Kaplan E. Receptive fields of P and M ganglion cells across the primate retina. *Vision Res*. 1995;35:7–24.
87. Dacey DM, Petersen MR. Dendritic field size and morphology of midget and parasol ganglion cells of the human retina. *Proc Natl Acad Sci U S A*. 1992;89:9666–9670.
88. Volbrecht VJ, Shrago EE, Schefrin BE, Werner JS. Ricco's areas for S- and L-cone mechanisms across the retina. *Color Res Appl*. 2000;26:S32–S35.
89. Barlow HB. Retinal noise and absolute threshold. *J Opt Soc Am*. 1956;46:634–639.
90. Radhakrishnan H, Pardhan S. Contrast detection in noise with positive and negative defocus in myopes. *Vision Res*. 2006;46:2949–2955.
91. Liang B, Liu R, Dai Y, Zhou J, Zhou Y, Zhang Y. Effects of ocular aberrations on contrast detection in noise. *J Vis*. 2012;12.
92. Elliott DB, Gilchrist J, Whitaker D. Contrast sensitivity and glare sensitivity changes with three types of cataract morphology: are these techniques necessary in a clinical evaluation of cataract? *Ophthalmic Physiol Opt*. 1989;9:25–30.
93. Hess R, Woo G. Vision through cataracts. *Invest Ophthalmol Vis Sci*. 1978;17:428–435.
94. Drews-Bankiewicz MA, Caruso RC, Datiles MB, Kaiser-Kupfer MI. Contrast sensitivity in patients with nuclear cataracts. *Arch Ophthalmol*. 1992;110:953–959.
95. de Gracia P, Marcos S, Mathur A, Atchison DA. Contrast sensitivity benefit of adaptive optics correction of ocular aberrations. *J Vis*. 2011;11(12):5.
96. Liu R, Zhou J, Zhao H, et al. Immature visual neural system in children reflected by contrast sensitivity with adaptive optics correction. *Sci Rep*. 2014;4:4687–4687.

Investigative Ophthalmology & Visual Science

97. Kern TS, Barber AJ. Retinal ganglion cells in diabetes. *J Physiol*. 2008;586:4401–4408.
98. Pelli DG, Giglio A. What internal noise source limits peripheral vision?, *European Conference on Visual Perception*. Berlin, Germany: 2017.
99. Pelli DG, Yiltiz H. What internal noise source limits peripheral vision?. *Vision Sciences Society*. St. Pete Beach, Florida; 2017.
100. Schlamp CL, Li Y, Dietz JA, Janssen KT, Nickells RW. Progressive ganglion cell loss and optic nerve degeneration in DBA/2J mice is variable and asymmetric. *BMC Neurosci*. 2006;7:66.
101. Buckingham BP, Inman DM, Lambert W, et al. Progressive ganglion cell degeneration precedes neuronal loss in a mouse model of glaucoma. *J Neurosci*. 2008;28:2735–2744.
102. Weber AJ, Kaufman PL, Hubbard WC. Morphology of single ganglion cells in the glaucomatous primate retina. *Invest Ophthalmol Vis Sci*. 1998;39:2304–2320.
103. Gupta N, Yucel YH. What changes can we expect in the brain of glaucoma patients? *Surv Ophthalmol*. 2007;52(suppl 2):S122–S126.
104. Lawlor M, Danesh-Meyer H, Levin LA, Davagnanam I, De Vita E, Plant GT. Glaucoma and the brain: Trans-synaptic degeneration, structural change, and implications for neuroprotection. *Surv Ophthalmol*. 2018;63:296–306.
105. Nuzzi R, Dallorto L, Rolle T. Changes of visual pathway and brain connectivity in glaucoma: a systematic review. *Front Neurosci*. 2018;12:363.
106. Song Y, Mu K, Wang J, et al. Altered spontaneous brain activity in primary open angle glaucoma: a resting-state functional magnetic resonance imaging study. *PLoS One*. 2014;9:e89493.
107. Li T, Liu Z, Li J, et al. Altered amplitude of low-frequency fluctuation in primary open-angle glaucoma: a resting-state FMRI study. *Invest Ophthalmol Vis Sci*. 2014;56:322–329.
108. Swanson WH, Horner DG. Assessing assumptions of a combined structure-function index. *Ophthalmic Physiol Opt*. 2015;35:186–193.
109. Price DA, Swanson WH, Horner DG. Using perimetric data to estimate ganglion cell loss for detecting progression of glaucoma: a comparison of models. *Ophthalmic Physiol Opt*. 2017;37:409–419.
110. Raza AS, Hood DC. Evaluation of the structure–function relationship in glaucoma using a novel method for estimating the number of retinal ganglion cells in the human retina. *Invest Ophthalmol Vis Sci*. 2015;56:5548–5556.
111. Curcio CA, Allen KA. Topography of ganglion cells in human retina. *J Comp Neurol*. 1990;300:5–25.

Investigative Ophthalmology & Visual Science